J. Fluid Mech. (1989), *vol.* 206, *pp.* 171–191
Printed in Great Britain

Spin-up phenomena in non-axisymmetric containers

By G. J. F. VAN HEIJST

Institute of Meteorology and Oceanography, University of Utrecht, Princetonplein 5, Utrecht, The Netherlands

(Received 17 July 1988 and in revised form 6 March 1989)

The spin-up from rest of a contained homogeneous free-surface fluid has been examined in the laboratory for a variety of non-axisymmetric containers. It was found that in the spin-up process three stages can be distinguished before the fluid reaches the ultimate state of rigid-body rotation. When the container starts spinning, the non-axisymmetric lateral tank boundaries induce horizontal pressure gradients, and as a result relative flows arise instantaneously after the start of the experiment. The absolute vorticity of the starting flow is zero, and a description can be given in terms of potential theory. Theoretical solutions have been derived for a number of geometries, and comparison with experimentally observed streamline patterns shows good agreement. In the next stage, flow separation sets in, in most cases leading to locally intense three-dimensional turbulent flows. The basic rotation causes a transition from three-dimensional to two-dimensional motion, and a subsequent organization of the relative flow into a number of cells is observed. During the final stage, the flow in these cells gradually decays owing to the spin-up/spin-down mechanism provided by the Ekman layer at the bottom of each cell, until eventually the fluid is in solid-body rotation.

1. Introduction

The spin-up of a fluid in a rotating container is a fundamental problem in fluid mechanics, and has been studied under different conditions by a number of investigators. Apart from their practical engineering applications in for example turbomachinery, spin-up flows are relevant to geophysical and astrophysical fluid dynamics. A comprehensive review of theoretical and experimental work on spin-up flows is written by Benton & Clark (1974).

Most previous studies – if not all – considered the spin-up of a homogeneous or stratified fluid in axisymmetric containers, and attention was in particular focused on cylindrical and spherical geometries. A careful analysis of the flow arising in a closed rotating cylinder when its rotation speed Ω was instantaneously increased with a small amount $\Delta\Omega$, was given by Greenspan & Howard (1963). As a reaction to the increased rotation speed Ekman layers develop at the horizontal boundaries (being the bottom and the lid) in which the flow is directed radially outwards. This radial outflow is compensated by weak axial flows directed towards the Ekman layers, commonly referred to as the Ekman suction flow. The radial Ekman flows are deflected by the sidewall of the container, at which a Stewartson shear layer occurs. Besides carrying axial transports, this Stewartson layer provides a weak radial flow to the interior domain (i.e. the region outside the viscous layers), which balances the axial flow towards the Ekman boundary layers. This (secondary) circulation in the

meridional plane driven by the Ekman layers brings interior fluid from larger radii to smaller radii, and thus provides an efficient spin-up mechanism: in order to conserve its angular momentum, the fluid in a ring of decreasing radius acquires a larger azimuthal velocity. Greenspan & Howard (1963) have analysed this time-dependent flow problem and they found that the time for the fluid to spin up, i.e. to reach the new state of rigid-body rotation with angular velocity $\Omega + \Delta\Omega$, is approximately given by $H/(\nu\Omega)^{\frac{1}{2}}$, with H the cylinder height, ν the kinematic fluid viscosity, and Ω the initial rotation speed of the cylinder. This spin-up time is usually short compared with the 'viscous' timescale H^2/ν, which is – in most practical situations – larger by one or two orders of magnitude. The analysis was carried out for the linear case, in which the speed increase was small enough ($\Delta\Omega/\Omega \ll 1$) so that the nonlinear advection terms in the equation of motion could be neglected. Later analyses revealed, however, that the timescale for the linear spin-up also applies to the nonlinear case, in which $\Delta\Omega$ is no longer small compared with Ω. Surprisingly, this timescale was also found to apply to the spin-up from rest. Although these results concern spin-up flows in an axisymmetric container with a rigid lid, the symmetry about the half-plane allows a direct translation to the case of a free-surface fluid in a cylinder, assuming that surface elevations have negligible effect on the flow dynamics.

In the case where the fluid is stratified, the spin-up becomes more complicated because the density gradients will affect the secondary circulation driven by the Ekman layers at the horizontal boundaries. The linear spin-up of a linearly stratified fluid in a closed cylinder has been studied by Walin (1969), who found that, although the flow arising after the speed increase of the cylinder is essentially different from that in the homogeneous case, the spin-up timescale to reach a 'final' state is the same as for a homogeneous fluid. This 'final' state is one of spatially non-uniform rotation, and the ultimate state of uniform rotation is only achieved on the diffusive timescales associated with density and momentum diffusion. Buzyna & Veronis (1971) have conducted laboratory experiments on spin-up of a continuously stratified fluid, and Walin's theoretical results were found to be in reasonable accordance with their observations. The spin-up of a two-layer fluid has been examined theoretically and experimentally by Holton (1965) and Pedlosky (1967), by considering two layers of comparable depth, with the interface not touching or intersecting the bottom of the container. It was found by Linden & van Heijst (1984) that, for the case of a shallow lower layer, intersection of the interface with the bottom results in the formation of a density front, which further complicates the spin-up of both layers. An important factor in these stratified spin-up problems is the occurrence of baroclinic instabilities, which give rise to wave-like, non-axisymmetric motions. Such motions decay extremely slowly, so that the timescale for the fluid to adjust to the increased rotation speed of the container is much larger than for baroclinically stable flows.

As stated before, most previous spin-up studies were concerned with flows in axisymmetric containers. The present study addresses the problem of the nonlinear spin-up from rest of a homogeneous free-surface fluid in a variety of non-axisymmetric containers. The geometries considered here are: (i) an annular region between two coaxial cylinders with a radial barrier between the cylinder walls; (ii) a semicircle region; (iii) a circular region with a radial barrier extending from the centre to the tank wall; and (iv) a region enclosed by two non-concentric cylinders connected by a radial barrier. The non-axisymmetry of the flow geometry gives rise

to complicated time-dependent flow structures, and it was found that in the spin-up process three main stages can be distinguished. Laboratory experiments revealed that the flow arising instantaneously after the tank starts rotating still has zero absolute vorticity, and its structure can thus be calculated by potential theory. Owing to the geometry, this starting flow is essentially non-axisymmetric. In the next stage of the spin-up process, flow separation occurs, leading to irregular flow patterns. In the next stage, organization of the relative flow into regular cell patterns is observed, an effect caused by the two-dimensional nature of the motion in this particular stage. These patterns are persistent, while the flow in each cell slowly decays by the well-known spin-up/spin-down mechanism associated with the Ekman layer present at the bottom of each cell, in analogy with the spin-up of a homogeneous fluid in an axisymmetric rotating cylinder.

The flows in the various geometries have been studied both experimentally and theoretically. Section 2 focuses on the annular geometry with a radial barrier, whereas the other geometries (ii), (iii) and (iv) are considered in §3. Finally, some general conclusions are formulated in §4.

2. Fluid in an annulus with a radial barrier

Consider the following configuration of a Newtonian fluid confined in an annular region between two coaxial cylinders, with a radial barrier extending from the inner cylinder to the outer cylinder, thus making the region 'singly connected'. The fluid has a free surface, and its depth is denoted by H. The diameters of the outer and the inner cylinder walls are given by D_0 and D_1, respectively. This system of cylinders and radial wall is mounted on a turntable in such a way that the rotation axis coincides with the cylinder axis. The rotation speed Ω of the turntable can be varied continuously from 0 to approximately 2 rad s^{-1}; the speed is controlled by an electronic feedback circuit and kept at a constant value within 0.5% accuracy. Initially, $\Omega = 0$ and the fluid is completely at rest. At $t = 0$ the table starts rotating, its angular speed gradually being brought to some value $\Omega > 0$. The acceleration of the table itself typically takes 3–5 s, depending on the ultimate Ω-value. The starting flow as well as the fluid flow in later stages of the spin-up process is visualized by small tracer particles floating on the free surface; their motion is recorded by a corotating photocamera mounted at some distance above the fluid. For the purpose of contrast enhancement, the fluid (ordinary tap water) was dyed with potassium permanganate or with methylen blue. Streamlines were visualized by making time exposures, and in a number of experiments velocity distributions were determined by measuring streak lengths.

2.1. *Description of the spin-up flow*

Immediately after starting the turntable, the fluid is pushed forward by the radial barrier: the pressure on the 'push-side' of the barrier rises, while it drops at its rear, thus creating an azimuthal pressure gradient which drives a considerable prograde flow (i.e. in the same sense as the table rotation) along the inner cylinder wall, directed from the higher to the lower pressure region. At the same time a retrograde return flow occurs along the outer wall, as schematically depicted in figure 1(*a*). Streamlines take on the appearance of a single closed cell, which fills the entire annular region. When the table is started too abruptly, gravity waves may be generated that lead to oscillatory fluid motions. Such oscillations were avoided by

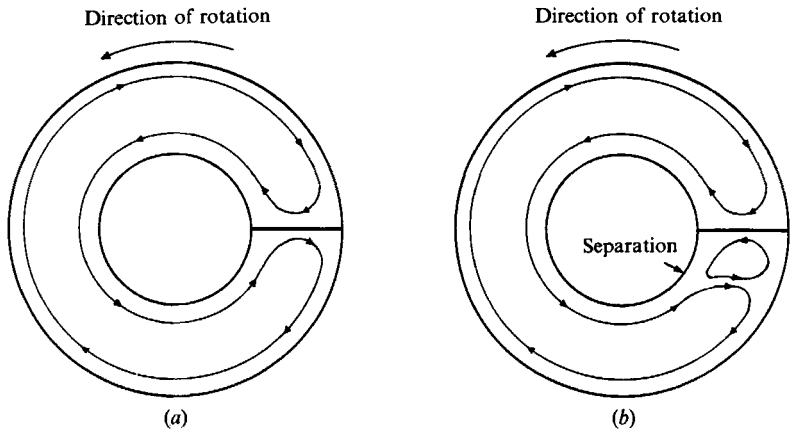

FIGURE 1. Schematic drawing of (*a*) the instantaneously arising starting flow, and (*b*) the subsequent flow separation (indicated by an arrow) in the annular flow geometry with a radial barrier.

spinning up the turntable more gently, and a streamline pattern was observed as shown in figure 2(*a*). Conservation of vorticity implies that this impulsively started flow is characterized by zero absolute vorticity.

Within typically 1 rotation period the pressure difference across the radial barrier vanishes (when the table is no longer accelerated), thus reducing the azimuthal pressure gradient to zero. As a consequence, the prograde flow is no longer able to follow the curved inner channel wall, and flow separation occurs, as depicted in figure 1(*b*). This phenomenon is clearly seen in figure 2(*b*), where the prograde jet-like flow separates from the inner cylinder wall, giving rise to a second, smaller cell with cyclonic circulation. The separation point moves gradually upstream (i.e. in a clockwise direction), and the separated jet-like flow thus induces an irregular, turbulent motion in the entire annular region. In this stage of the spin-up, both large-scale and vigorous small-scale eddy motions are observed in the fluid, giving the flow a rather chaotic turbulent appearance (see figure 2*c*).

After some more rotation periods the flow is seen to become organized into a more or less regular array of closed cells, as is clearly shown by figure 2(*d*). These cells, with alternately cyclonic and anticyclonic circulation, appear to be rather stable, and the associated relative flow decays slowly by frictional effects (mostly confined to the bottom Ekman layer), until an ultimate state of rigid-body rotation is reached.

The organization of the flow into a regular cell pattern is a result of the two-dimensionality of the flow, which causes energy transfer from smaller scales to larger scales (see Batchelor 1969). This phenomenon is commonly known as the 'inverse energy cascade' in two-dimensional turbulence. In order to understand this phenomenon, careful observations were carried out during the spin-up process, using floating tracer particles to visualize the surface motion, and neutrally buoyant particles for visualization of the fluid motion at lower levels. The observations revealed that, immediately after separation occurred at the inner sidewall, the turbulent flow was essentially three-dimensional within the entire domain. Within typically 2–4 rotation periods, however, the flow was seen to become nearly two-dimensional, the (horizontal) motion at lower levels being approximately identical to the motion at the free surface. This effect is caused by the system rotation, as expressed by the well-known Taylor–Proudman theorem. At this stage it was

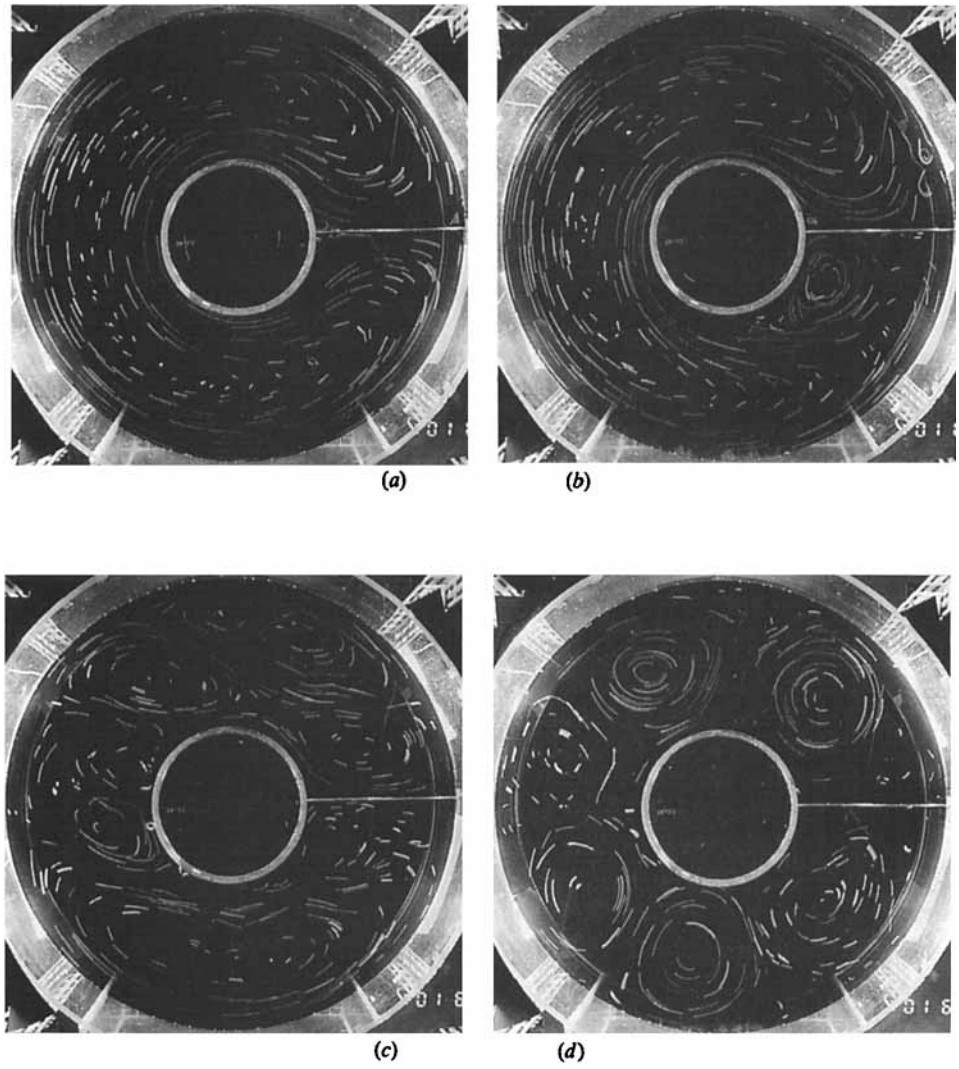

FIGURE 2. A sequence of photographs showing streaklines in four stages of the spin-up process in the annular geometry. Initially, the starting flow has the appearance of a single cell (*a*), and when flow separation occurs (*b*), the motion becomes irregular (*c*), until eventually the flow is observed to become organized into a regular array of cells (*d*). Experimental parameters are: $H = 18.5$ cm, $\Omega = 0.755$ rad/s, $D_o = 92.5$ cm, $D_i = 30.0$ cm. The photographs were taken at (*a*) $t = 0.4T$, (*b*) $1.0T$, (*c*) $3.0T$ and (*d*) $10.8T$, with $T = 8.3$ s the rotation period. The exposure time of the photographs (*a–c*) was 1 s, whereas the exposure time of (*d*) measured 2 s.

observed that smaller eddies grow and merge with others, thus demonstrating the existence of the inverse cascade of kinetic energy. The width of the channel puts a physical limit on the ultimate eddy size, so that eventually the cells are arranged in a regular array filling the channel over its full length.

2.2. *Analysis*

2.2.1. *The flow in the initial stage*

As the fluid is initially at rest, the flow arising immediately after starting the turntable will still have zero absolute vorticity. The vorticity of the relative flow (as

observed by the corotating photocamera) is therefore -2Ω, with Ω the table rotation speed at that particular instant. Assuming that the motion in this stage is two-dimensional, i.e. surface elevations and depressions are small compared with the fluid depth H, the relative flow can be represented by a two-dimensional stream function Ψ, which thus has to satisfy $\nabla^2\Psi = 2\Omega$. The stream function Ψ is here defined by $\boldsymbol{v} = -\hat{\boldsymbol{k}} \times \nabla\Psi$, with $\hat{\boldsymbol{k}}$ the unit vector in the axial (i.e. vertical) direction, and $\boldsymbol{v}$ the (horizontal) velocity vector. Although viscous layers develop at the solid boundaries, their presence can be neglected in this initial stage, so that to a good approximation $\Psi = 0$ at the lateral flow boundaries.

In view of the geometry of the flow region a cylindrical coordinate system (r, θ) is introduced, with r the radius measured from the geometric centre and θ the azimuthal angle. One side of the radial barrier corresponds with $\theta = 0$, its rear side with $\theta = 2\pi$. When lengths are scaled by the tank radius, the outer and inner channel walls are given by $r = 1$ and $r = a$, respectively. The flow problem can then be formulated as

$$\nabla^2\Psi(r, \theta) = 2\Omega, \tag{1}$$

with

$$\left.\begin{array}{lll} a \leqslant r \leqslant 1; & \theta = 0, 2\pi: & \Psi = 0, \\ r = a, 1; & 0 \leqslant \theta \leqslant 2\pi: & \Psi = 0. \end{array}\right\} \tag{2}$$

A particular solution of (1) is

$$\Psi_{\mathrm{p}}(r, \theta) = \Omega r^2 \sin^2\theta, \tag{3}$$

so that the resulting homogeneous problem becomes

$$\nabla^2\Psi(r, \theta) = 0, \tag{4}$$

with

$$\left.\begin{array}{lll} a \leqslant r \leqslant 1; & \theta = 0, 2\pi: & \Psi = 0, \\ r = a; & 0 \leqslant \theta \leqslant 2\pi: & \Psi = -\Omega a^2 \sin^2\theta, \\ r = 1; & 0 \leqslant \theta \leqslant 2\pi: & \Psi = -\Omega \sin^2\theta. \end{array}\right\} \tag{5}$$

It is convenient to transform this problem to the half-circle geometry by

$$r = s^2, \quad \theta = 2\alpha, \tag{6}$$

in which $a^{\frac{1}{2}} \leqslant s \leqslant 1$ and $0 \leqslant \alpha \leqslant \pi$. The general solution of $\nabla^2\Psi(s, \alpha) = 0$ is

$$\Psi(s, \alpha) = (A \cos n\alpha + B \sin n\alpha)(C/s^n + Ds^n) + A_0 \ln s + B_0, \tag{7}$$

with n an integer; A, B, C and D are coefficients to be determined from the boundary conditions (5), which have to be transformed to the (s, α)-coordinates according to (6). Application of these conditions at $r = a$ and $r = 1$ requires a series representation of $\sin^2 2\alpha$, which can be obtained by standard Fourier series theory. For $\sin^2 k\alpha$, with k a positive integer, this yields

$$\sin^2 k\alpha = -\frac{8k^2}{\pi} \sum_{n=1}^{\infty} \frac{\sin n\alpha}{(n-2k)n(n+2k)} \quad (n \text{ odd}, \quad 0 \leqslant \alpha \leqslant \pi). \tag{8}$$

One thus finds the solution $\Psi(s, \alpha)$ on the half-circle geometry, and by the inverse transformation $(s, \alpha) \to (r, \theta)$ the solution for the stream function $\Psi(r, \theta)$ in the original geometry is found to be

$$\Psi(r, \theta) = \Omega r^2 \sin^2\theta + \frac{32\Omega}{\pi} \sum_{n=1}^{\infty} \left[a^2 \left\{ \left(\frac{1}{r}\right)^{n/2} - r^{n/2} \right\} + \left(\frac{r}{a}\right)^{n/2} - \left(\frac{a}{r}\right)^{n/2} \right] \times [a^{-n/2} - a^{n/2}]^{-1} \frac{\sin \frac{1}{2}n\theta}{(n-4)n(n+4)} \quad (n \text{ odd}). \tag{9}$$

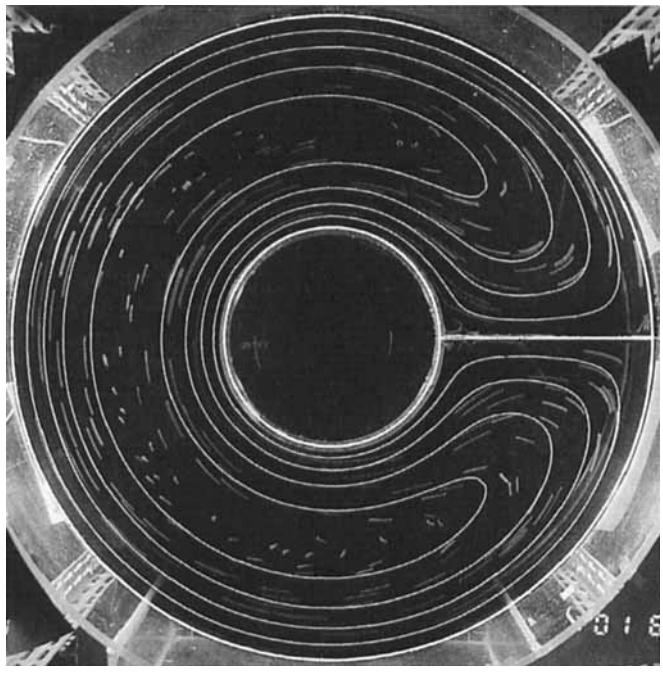

FIGURE 3. Comparison of the theoretical streamline pattern according to (9) for $\Psi = 0, -0.025, \ldots, -0.10$ and the experimentally observed starting flow (as shown in figure 2*a*) in the annular geometry.

A number of streamlines $\Psi =$ constant were plotted and projected on the single-cell flow as observed by the photocamera (see figure 2*a*) in the initial phase of the spin-up process. The result is presented in figure 3, and it is clear that the theory fits the observation very well.

The azimuthal velocity $v_\theta(r, \theta)$ in the flow field can be deduced from (9) by differentiating Ψ according to $v_\theta = -\partial\Psi/\partial r$, yielding

$$v_\theta(r,\theta) = -2\Omega r \sin^2\theta + \frac{16\Omega}{\pi}\sum_{n=1}^{\infty}\left[a^2\left\{\left(\frac{1}{r}\right)^{n/2} + r^{n/2}\right\} - \left(\frac{r}{a}\right)^{n/2} - \left(\frac{a}{r}\right)^{n/2}\right] \times\left[\left(\frac{1}{a}\right)^{n/2} - a^{n/2}\right]^{-1} r^{-1}\frac{\sin\frac{1}{2}n\theta}{(n-4)(n+4)} \quad (n \text{ odd}). \quad (10)$$

In a number of experiments the azimuthal velocity at $\theta = \pi$ was measured from the streak lengths at different radii. A typical example of the radial distribution of $v_\theta(\theta = \pi)$ is shown in figure 4, in which the dots represent experimental data, and the solid curve represents the theoretical velocity profile $v_\theta(r, \pi)$ according to (10). It must be noted that the streak lengths were measured while the table was still spinning up from 0 to its ultimate rotation speed Ω, and unfortunately the exact value of the rotation speed at the moment the photograph was taken is not known. For this reason the amplitude of the theoretical v_θ-profile was decreased, until it matched the amplitude of the measured profile. Nonetheless, the radial structures of both profiles agree very well.

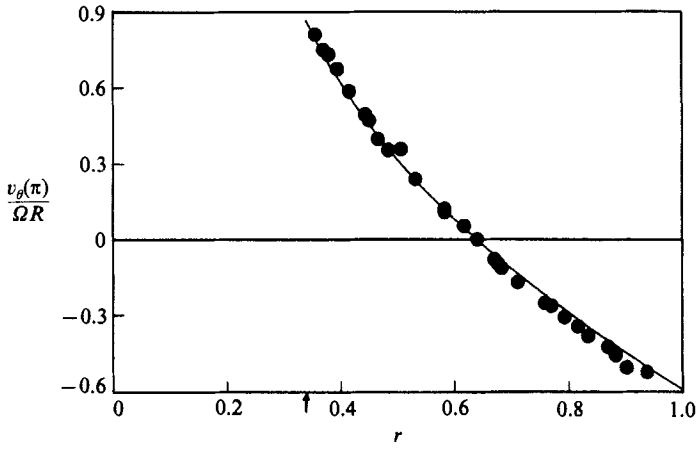

FIGURE 4. Radial distribution of the azimuthal velocity at $\theta = \pi$ in the annular geometry immediately after starting the turntable. The dots represent the experimental data obtained from the observed streak lengths, whereas the solid line represents the theoretical solution for $v_\theta(\theta = \pi)$ according to (10). The radial coordinate and the velocity magnitude are scaled by R and ΩR, respectively, with R the tank radius and Ω the ultimate rotation speed of the turntable. The arrow indicates the position of the inner wall. Experimental parameters: $H = 18.4$ cm, $\Omega = 0.84$ rad/s, $D_o = 92.5$ cm, $D_i = 30.0$ cm.

2.2.2. *The number of cells*

The beginning of this section contained a description of how flow separation at the inner channel wall sets in, and the eventual organization of the resulting irregular flow into a regular pattern of cells (see figure 2*d*). It was argued that the channel width puts a limit on the cell size and, assuming that the cells tend to be roughly circular, this implies that their number increases with a decreasing channel width. Under the assumption of circular cells, their approximate number N will thus be given by

$$N = env\left(\frac{D_o + D_i}{D_o - D_i}\pi\right), \tag{11}$$

with D_o and D_i the diameters of the outer and the inner channel walls, respectively.

In order to verify this conjecture a number of experiments were carried out in which the inner diameter D_i was varied from 12.0 cm to 51.0 cm (in all the experiments the outer diameter D_o was kept at 92.5 cm). It was indeed found that the number of cells is larger in a narrower channel, as illustrated by figure 5. This photograph shows the ultimate streamline pattern in a channel with $W = \frac{1}{2}(D_o - D_i) = 21.0$ cm, in which 11 cells can be distinguished, in contrast to $N = 6$ in the case $W = 31.3$ cm (figure 2*d*). The observed values of N are presented graphically as a function of D_i in figure 6. The step-like solid line represents the conjectural relationship (11) between N and D_i, and the agreement with the experimental data (denoted by black dots) appears to be good. In a number of experiments the number of cells jumped between two neighbouring integer values, and for these cases the corresponding dots are connected by a solid vertical line. Although both the ultimate rotation speed Ω and the water depth H were varied in the experiments (in the ranges 0.44–1.14 rad s^{-1} and 7.2–24.1 cm, respectively), the number N did not appear to be dependent on these parameters. Nonetheless, Ω and H do play an important role in the spin-up process, viz. in the decay of the cell vortices.

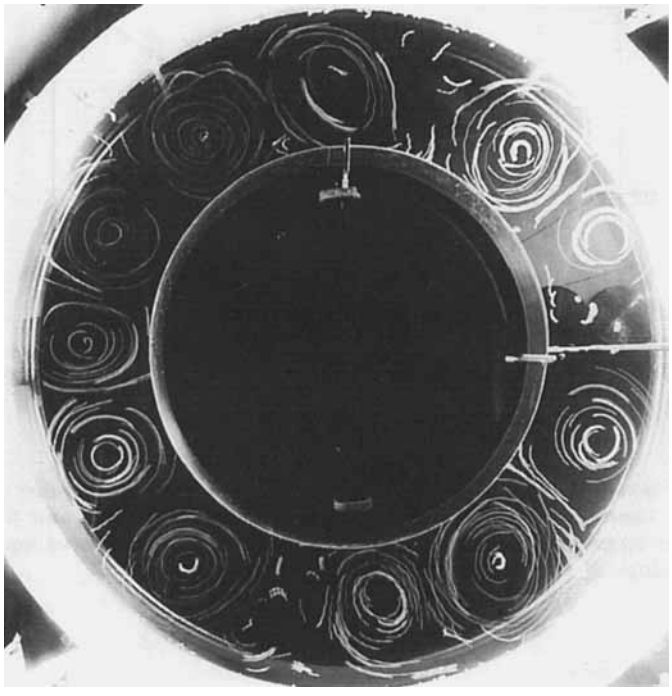

FIGURE 5. Streakline photograph showing 11 cells in the final stage of the spin-up in the annular geometry, with a narrower channel than the one in figure 2. Experimental parameters: $H = 15.2$ cm, $\Omega = 1.00$ rad/s, $D_o = 92.5$ cm, $D_i = 50.0$ cm.

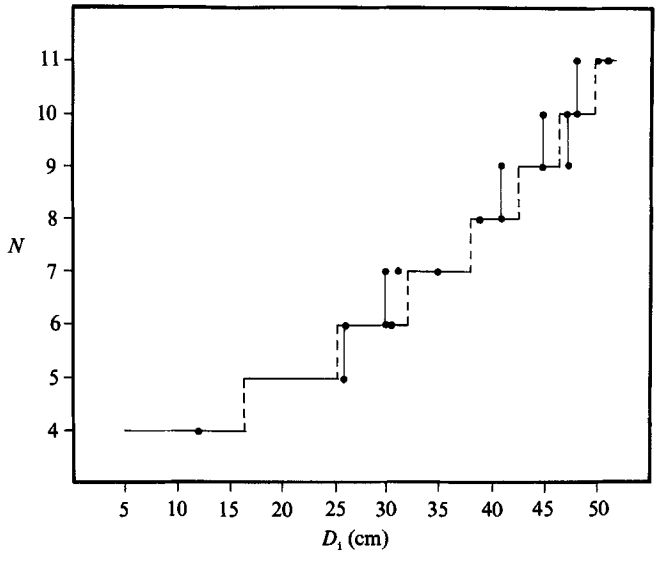

FIGURE 6. Graph showing the relationship between the number N of cells and the channel width $\frac{1}{2}(D_o - D_i)$. The dots represent data obtained in laboratory experiments in which D_i varied from 12.0 cm to 51.0 cm, while D_o was kept at 92.5 cm. The step-like solid curve represents the conjectural relationship (11) between N and D_i.

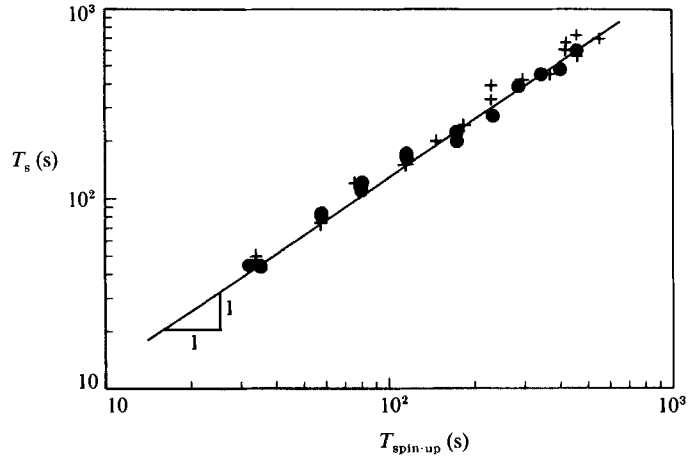

FIGURE 7. Comparison of the spin-up timescale T_s according to (13) and a number of experimentally observed spin-up times for the annular geometry (indicated by dots) and for the semicircle geometry shown in figure 9(*a*) (data indicated by plus signs). The solid curve represents a fit with a straight line of slope 1.

2.2.3. *The spin-up time*

Once the flow has become organized into a regular array of roughly circular vortices, its structure does not show any drastic changes. On the contrary, the relative fluid motion is seen to decay very slowly, until the ultimate state of solid-body rotation, i.e. zero relative flow, is reached. It seems reasonable to assume that in this final stage of the spin-up process frictional effects are mainly confined within an Ekman layer at the bottom of each cell. This Ekman boundary layer plays a crucial part in the spin-up or spin-down of the cells, much more than the frictional shear layers at the lateral boundaries. The linear and nonlinear spin-up of fluid in a circular cylinder has been investigated extensively (see e.g. Greenspan & Howard 1963). It was found that the characteristic timescale for this spin-up in a closed container of height $\bar{H}$ is

$$T_s^* = (\Omega E^{\frac{1}{2}})^{-1}, \tag{12}$$

where E is the Ekman number defined as $\nu/(\Omega\bar{H}^2)$, with ν the kinematic fluid viscosity. This spin-up mechanism is also responsible for the flow decay in the cell pattern, but because of the free surface – which is assumed to be free of any shear stresses – the appropriate spin-up timescale for this case is

$$T_s = 2H/(\nu\Omega)^{\frac{1}{2}}, \tag{13}$$

with H the depth of the fluid column. Figure 7 shows a comparison of experimentally observed spin-up times (measured from the start of each experiment) and this Ekman timescale T_s. The black dots represent data obtained for the annular geometry with a radial wall, while the plus signs refer to a different flow geometry, to be discussed in the next section. In most experiments only the water depth H was changed (from 1.5 cm to 20.0 cm) while the other parameters were kept constant, but in a few additional runs both the rotation speed Ω and the water depth H were varied. All the dots seem to collapse on a straight line of slope 1, indicating that the decay time of the flow in the present geometry is indeed given by (13).

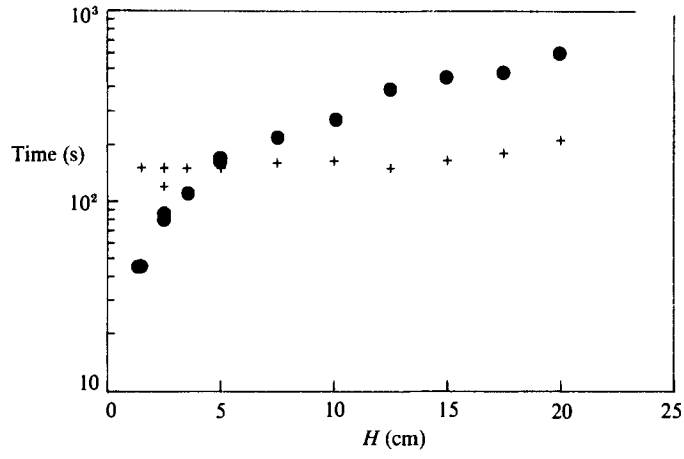

FIGURE 8. Graph of observed spin-up (dots) and spin-down (plus signs) times for fluid in the annular geometry as a function of the depth H. The other experimental parameters were kept constant, viz. $\Omega = 0.755$ rad/s, $D_1 = 30.0$ cm and $D_0 = 92.5$ cm.

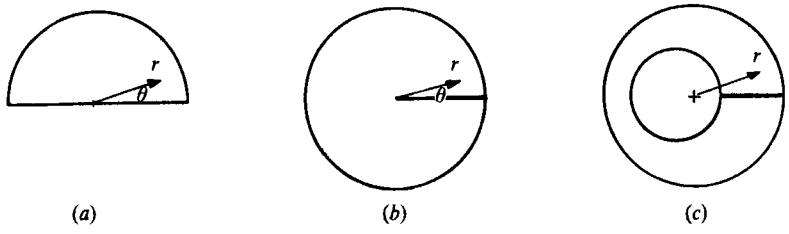

FIGURE 9. Flow geometries considered in §3: (*a*) the semicircle, (*b*) the circular region with a radial barrier, and (*c*) the region enclosed by two non-concentric cylinders and a radial barrier.

Thus far, attention has been focused on the spin-up of the fluid from rest, but an equally intriguing question concerns the spin-down of the fluid in this geometry from solid-body rotation at speed Ω to rest. In order to investigate the spin-down flow, some 15 experiments were carried out in which – after the fluid was brought to solid-body rotation – the table rotation speed Ω was gradually reduced to zero. Initially one observes the same flow behaviour as shown in figure 2(*a*), only with the flow directions reversed: there is a strong retrograde flow along the inner channel wall, compensated by a prograde backflow along the outer wall. As in the spin-up case (figure 2*b*), flow separation sets in very quickly. The separating wall current again induces a three-dimensionally turbulent flow in the entire fluid region, but – in contrast to the spin-up case – the flow shows no tendency whatsoever to become two-dimensional: it keeps its three-dimensional character until it has acquired the ultimate state of rest. For this reason no organization into cells is observed, and the flow remains irregular while decaying.

A comparison between spin-up times and spin-down times for this particular geometry is presented in figure 8. In these experiments the water depth was changed systematically from 1.5 cm to 20.0 cm, with the other parameters held at a constant value. As can be expected from (13) the spin-up time increases proportionally with the depth H, but the spin-down time seems to take a constant value, independent of H, only showing a slight increase at larger H-values.

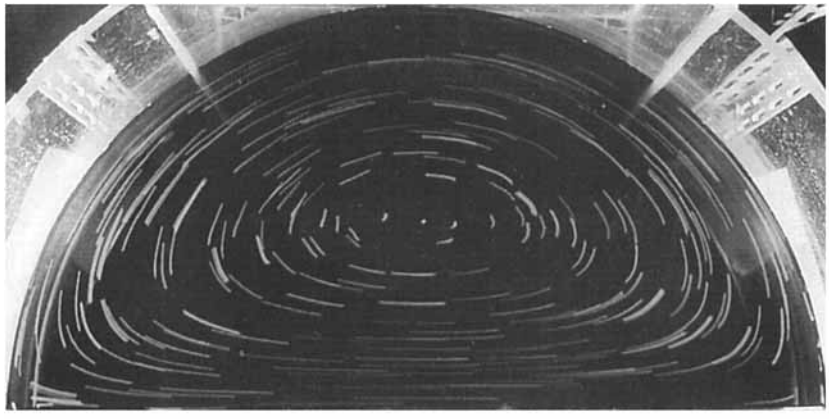

(a)

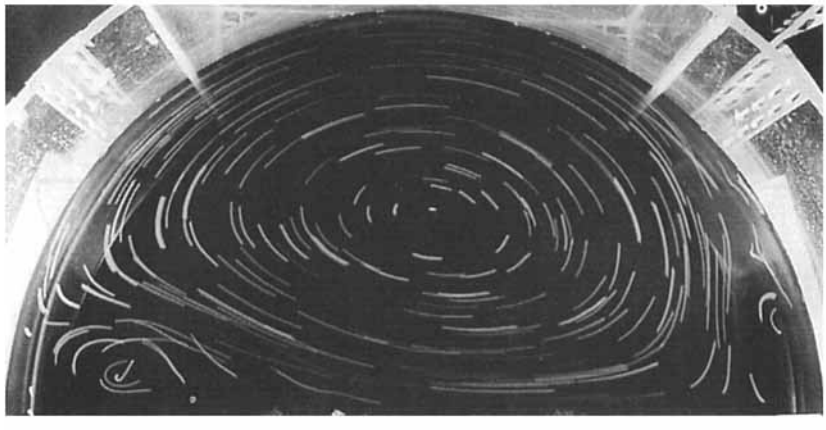

(b)

(c)

FIGURE 10 (a–c). For caption see facing page.

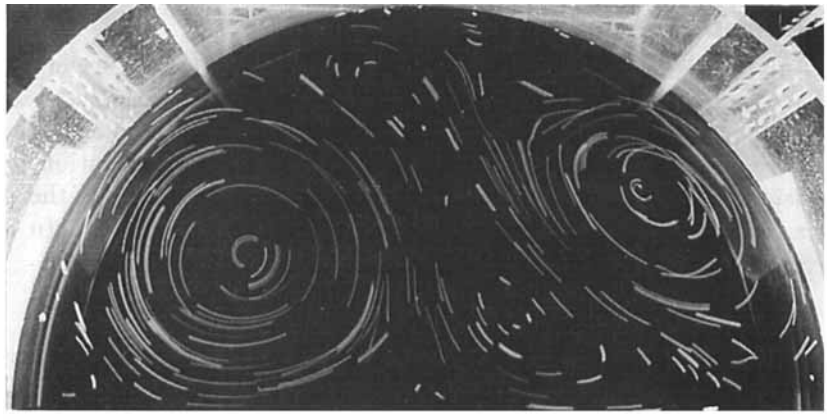

(*d*)

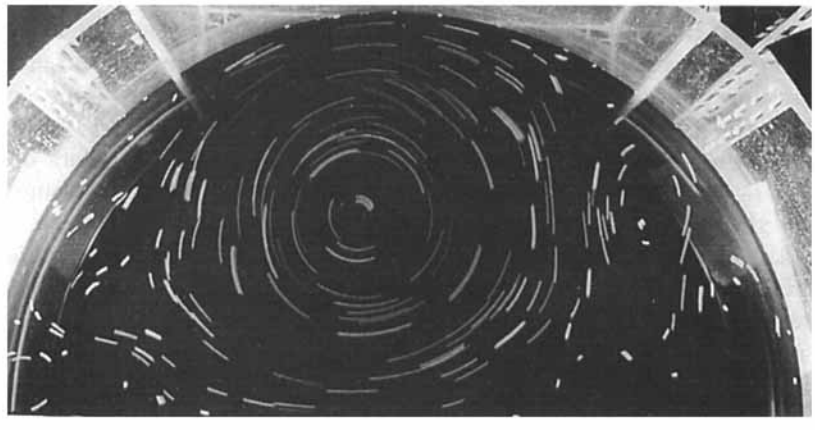

(*e*)

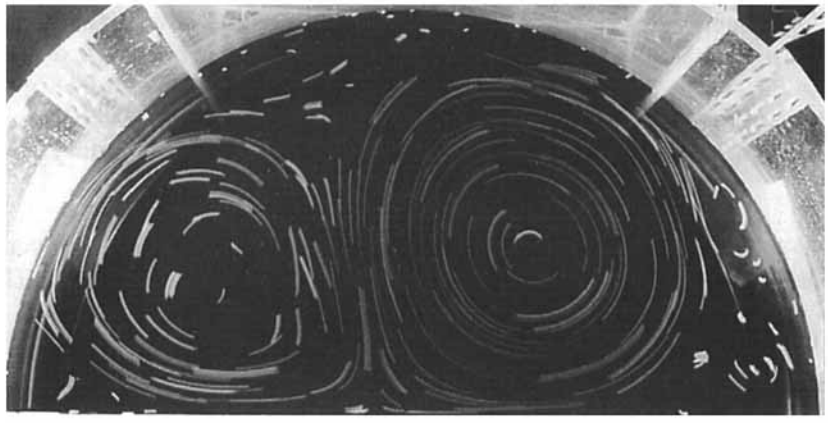

(*f*)

FIGURE 10. Sequence of streakline photographs showing the evolution of the relative flow during the spin-up in the semicircle geometry, taken at (*a*) $t = 0.4T$, (*b*) $1.0T$, (*c*) $1.8T$, (*d*) $2.4T$, (*e*) $5.4T$, and (*f*) $14.4T$, with $T = 8.3$ s the rotation period. The exposure time of (*a–e*) was 1 s, whereas the exposure time of (*f*) measured 3 s. Experimental parameters: $H = 12.5$ cm, $\Omega = 0.756$ rad/s.

3. Other geometries

The spin-up of a free-surface fluid has also been studied in a number of other non-axisymmetric geometries, which are depicted schematically in figure 9: the semicircle (a), the circular region with a single radial barrier (b), and the region enclosed by two non-concentric cylinders connected by a radial barrier (c). Configuration (b) can in fact be considered as a limiting case of the geometry considered in the previous section, viz. with the inner cylinder radius approaching zero ($a \to 0$). In all these cases the centre ($r = 0$) of the container coincides with the rotation axis.

3.1. *The semicircle geometry*

Immediately after starting the turntable, the pressure at $\theta = 0$ rises, whereas it drops at $\theta = \pi$. As a result, an intense flow develops instantaneously along the flat boundary, directed from ($r = 1$, $\theta = 0$) to ($r = 1$, $\theta = \pi$). An additional backflow arises along the curved boundary, so that the streamlines have the appearance of closed cells with anticyclonic circulation. Particle paths photographed in this initial stage of the spin-up clearly illustrate the shape of the streamlines (see figure 10a). Within one revolution of the turntable the pressure gradient along the flat boundary is considerably reduced (because the table is no longer accelerated) and, in addition, shear layers develop at the lateral boundaries in which locally cyclonic vorticity is generated. Both effects cause the main flow to separate from the walls, leading to the formation of two smaller cells with cyclonic circulation in the corners of the flow domain (see figure 10b). The subsequent photographs of the streamline patterns reveal that the sizes of the cyclonic corner vortices increase (figure 10c), and eventually the central anticyclonic cell is pinched (figure 10d) in such a way that it finally vanishes completely, leading to the merging of the two corner vortices. This stage is illustrated by figure 10(e), showing a single, cyclonic vortex in the centre of the flow region. As time progresses, a second cell with anticyclonic circulation develops in the corner region ($r = 1$, $\theta = \pi$), and its size increases gradually until – in the final state – the cyclonic and anticyclonic cells are of approximately equal size, filling the flow region completely. This combination of two cells appears to be rather stable, and the flow structure does not change very much during the decay until the ultimate state of solid-body rotation is reached.

As in the geometry discussed in the previous section, the flow in the initial stage of the spin-up process, i.e. immediately after starting the turntable, is described by $\nabla^2 \Psi(r, \theta) = 2\Omega$, with $\Psi = 0$ at the domain boundaries. Again, by adopting the particular solution $\Psi_p(r, \theta) = \Omega r^2 \sin^2\theta$, the problem becomes homogeneous; the Laplace equation $\nabla^2 \Psi(r, \theta) = 0$ has to be solved subject to the boundary conditions

$$\Psi(\theta = 0, \pi) = 0, \quad \Psi(r = 1) = -\Omega \sin^2\theta. \tag{14}$$

The general solution of this problem is – after replacing (s, α) by (r, θ) – given by (7), and the coefficients are determined by applying the boundary conditions (14). The condition at $r = 1$ requires a Fourier sine series representation, which can be obtained by using (8) with $k = 1$. One thus finds the following complete solution:

$$\Psi(r, \theta) = \Omega r^2 \sin^2\theta + \frac{8\Omega}{\pi} \sum_{n=0}^{\infty} \frac{r^{2n+1} \sin(2n+1)\theta}{(2n-1)(2n+1)(2n+3)} \quad (0 \leqslant \theta \leqslant \pi). \tag{15}$$

A comparison between a number of streamlines Ψ = constant and the observed starting flow is presented in figure 11. It is clear that, apart from a slight shift, the

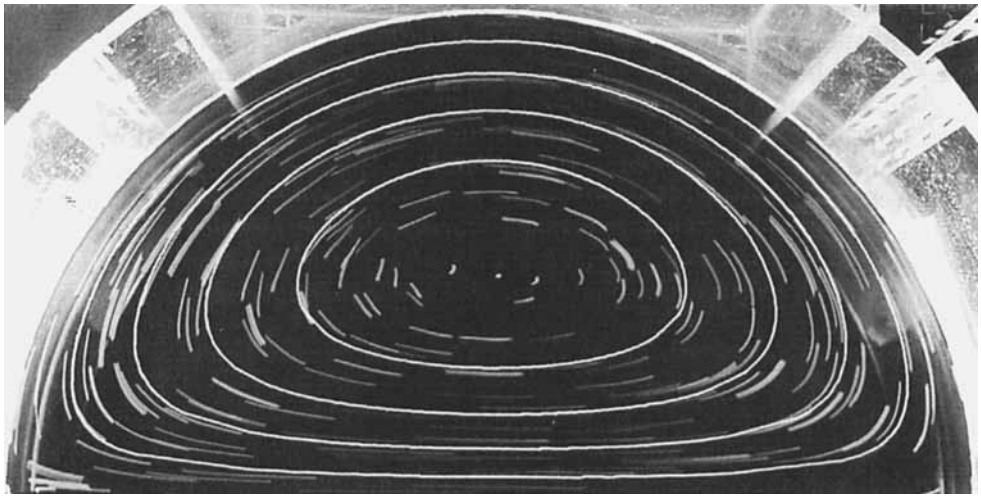

FIGURE 11. A comparison of the theoretical streamline pattern calculated according to (15) and the experimentally observed starting flow in the semicircle geometry. The streamlines are plotted for $\Psi = 0, -0.04, \ldots, -0.16$. Experimental parameters as in figure 10.

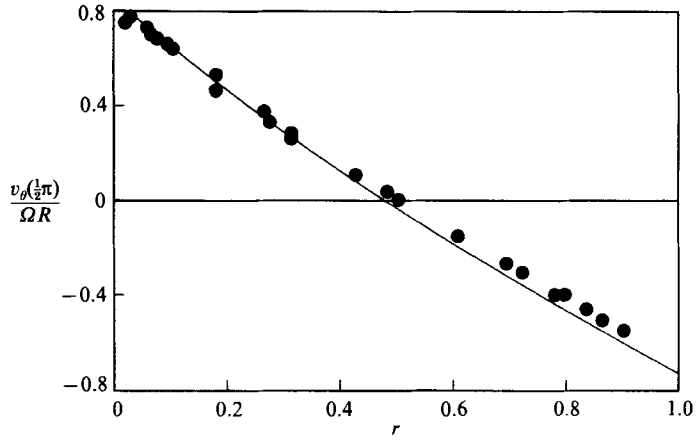

FIGURE 12. Radial distribution of the azimuthal velocity at $\theta = \frac{1}{2}\pi$ in the semicircle geometry immediately after starting the turntable. Experimental data are indicated by dots, whereas the solid line represents the theoretical solution $v_\theta(r, \frac{1}{2}\pi)$ according to (16). Scaling as in figure 4. Experimental parameters: $H = 20.0$ cm, $\Omega = 0.755$ rad/s.

theory fits the observation very well. A more quantitative comparison was made by measuring the radial distribution of the azimuthal velocity component $v_\theta(r, \theta)$ at $\theta = \frac{1}{2}\pi$ and comparing this with the theoretical profile. The azimuthal velocity is found from (15) by using $v_\theta = -\partial\Psi/\partial r$, which yields

$$v_\theta(r, \theta) = -2\Omega r \sin^2\theta - \frac{8\Omega}{\pi} \sum_{n=0}^{\infty} \frac{r^{2n} \sin(2n+1)\theta}{(2n-1)(2n+3)} \quad (0 \leqslant \theta \leqslant \pi). \tag{16}$$

Figure 12 shows the radial distribution of this theoretical solution v_θ at $\theta = \frac{1}{2}\pi$ (denoted by the solid line) as well as the experimentally determined velocity profile at $\theta = \frac{1}{2}\pi$ (denoted by black dots). As in figure 4, the amplitude of the theoretical

velocity profile was matched to that of the observed profile, because the velocity measurements were done while the table was still spinning up to its ultimate rotation speed, so that the exact value of Ω at the time of the photograph was not known. The agreement between theory and observation is quite good, although at larger radii the profiles are somewhat shifted. It could well be that this shift is caused by the non-uniform fluid depth in this initial stage: local changes in fluid depth cause additional advective flows as well as locally increased or decreased vorticity.

In 15 experimental runs the time was measured for the fluid to reach the ultimate state of solid-body rotation, and a comparison with the appropriate Ekman spin-up timescale T_s as defined by (13) is given in figure 7 (the data are indicated by plus signs). In these experiments only the water depth H was varied, from 1.5 cm to 24.1 cm, while the rotation speed was $\Omega = 0.755$ rad s^{-1} in all cases except one, in which it was 1.25 rad s^{-1}. The agreement with the Ekman timescale is good, which indicates that the decay of the two-cell flow in the 'final' state (shown in figure 10f) is caused by the spin-up/spin-down mechanism associated with the Ekman layers at the bottom of each cell.

3.2. *The circular region with a radial barrier*

As mentioned before, the circular geometry with a radial barrier shown in figure 9(b) can be considered as a limiting case of the flow configuration discussed in §2, with the radius of the inner cylinder approaching zero, i.e. $a \to 0$. When the turntable starts rotating, the fluid is observed to flow instantaneously from the 'push'-side of the barrier to its rear, while a compensating flow in an anticyclonic direction occurs along the cylinder wall. This starting flow is visualized in figure 13(a). Although this flow pattern resembles the motion observed in the annular geometry (figure 2a), flow separation was seen to occur almost instantaneously at the tip ($r = 0$) of the barrier. This is due to the (infinitely) small curvature of the barrier tip: owing to its inertia the fluid is not able to flow around the sharp 360° corner (this would require infinitely large accelerations), and a separation cell with cyclonic circulation is seen to arise near the rear side of the barrier tip. The size of this cell increases extremely quickly (figure 13b), and after roughly one revolution of the table three cells can be distinguished in the relative flow pattern (see figure 13c): one cell with cyclonic flow originating from the separation at the barrier tip, and two cells with slightly weaker anticyclonic flow. The final stage is reached after typically 5 rotation periods, and shows the occurrence of essentially four cells with alternately cyclonic and anticyclonic flow (see figure 13d). In comparison with the previous stage, the cell with cyclonic motion originating from the flow separation at the barrier tip has shifted in an anticyclonic direction, and sits in the upper left of the picture. In addition to the four main cells, some smaller cells are visible in the corners of the flow domain, on either side of the barrier. Apart from some minor changes in this relative flow pattern (shifting and deformation of the cells), the occurrence of four cells is persistent, and the relative motion in the cells slowly decays by the well-known spin-down/spin-up mechanism provided by the Ekman layers at the bottom of each cell.

Although separation sets in immediately after starting the turntable (figure 13a), it is tempting to compare the starting flow with the theoretical solution (9) in the limit $a \to 0$. For this limiting case a number of streamlines Ψ = constant are plotted in figure 14, and it is clear that – apart from the region near the edge of the barrier – this pattern very much resembles the observed flow shown in figure 13(a). The number of cells observed in the final stage ($N = 4$; see figure 13d) is not exactly in accordance with the conjectural relationship (11), which predicts $N = 3$ for the

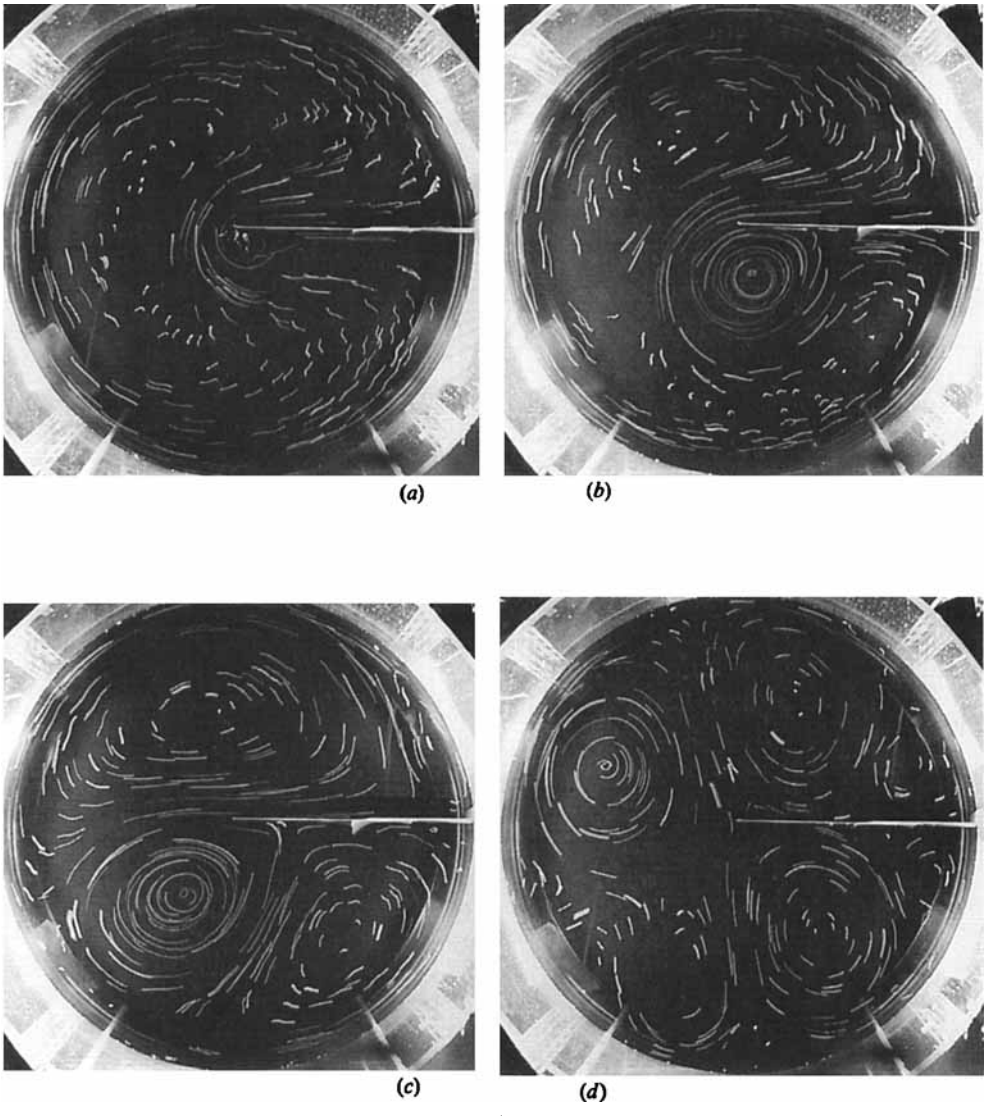

FIGURE 13. Sequence of streakline photographs showing the evolution of the relative flow during the spin-up in the circular geometry with a radial barrier, taken at (*a*) $t = 0.01T$, (*b*) $0.5T$, (*c*) $1.2T$, and (*d*) $4.8T$, with $T = 8.3$ s the rotation period. Exposure time: 1 s. Experimental parameters: $H = 12.5$ cm, $\Omega = 0.755$ rad/s.

extreme case $D_1 = 0$. However, this departure is attributed to the fact that (11) was derived for a curved channel of a width that is smaller than the radius of curvature, which is not the case for the geometry considered here.

3.3. *The region enclosed by two non-concentric cylinders with a radial barrier*

In the discussion of the flow in the annular region with a radial barrier (§2) it was mentioned that the size of the cells developing from the two-dimensional turbulent flow in the latter stages of the spin-up process was physically limited by the width of the channel. In the annular configuration the cells in the final flow stage are roughly equal in size, and their number N can to a good approximation be estimated

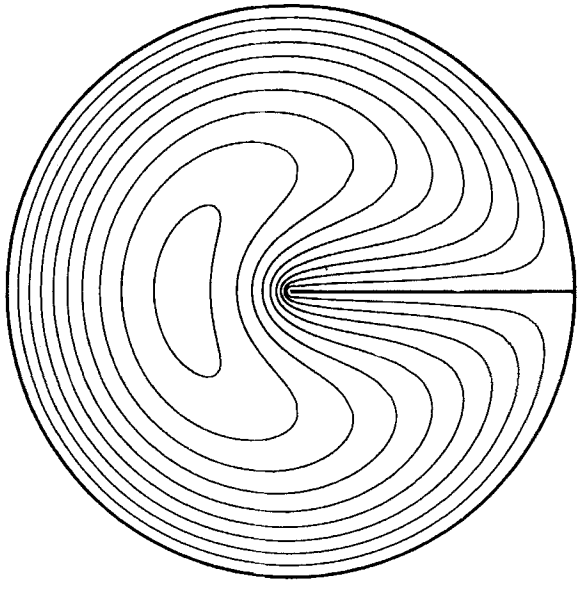

FIGURE 14. Streamlines for the circular geometry with a radial barrier calculated according to the theoretical solution (9) with $a = 0.01$. The streamlines are plotted for $\Psi = 0, -0.03, -0.06, \ldots, -0.27$.

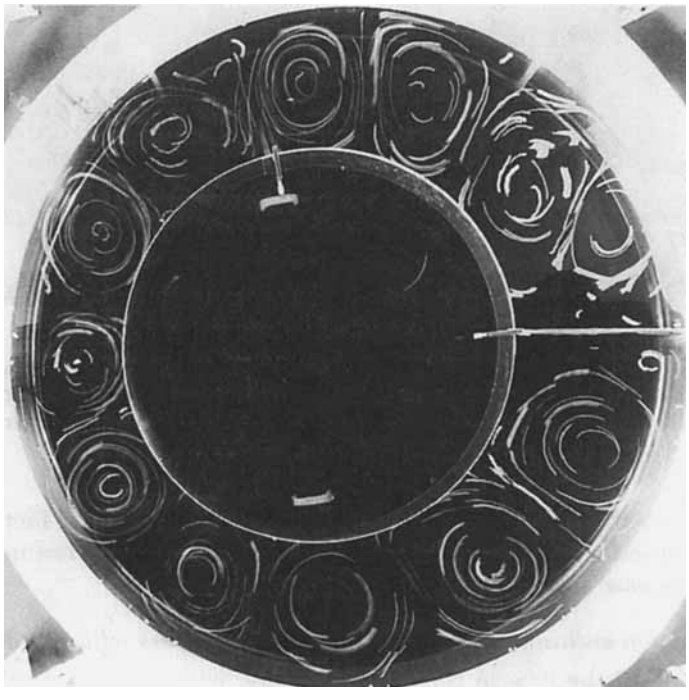

FIGURE 15. Streakline photograph showing the cell pattern in the final stage of the spin-up in the region between two non-concentric cylinders connected by a radial barrier. The inner cylinder has been shifted off-axis, so that the channel width varies between 17.5 cm and 26.0 cm. Experimental parameters: $H = 15.5$ cm, $\Omega = 1.00$ rad/s, $D_o = 92.5$ cm, $D_i = 49.0$ cm.

by geometrical arguments, see (11). This conjectural relationship was tested in a number of experiments, and the results presented in figure 6 indicate good agreement.

The dependence of the cell size on the channel width is nicely illustrated by spin-up experiments performed with fluid enclosed by two non-concentric cylinders connected by a radial barrier. In these experiments the axis of the outer cylinder coincided with the rotation axis, while the inner cylinder was shifted some distance δ off the rotation axis. The cylinders are connected by a radial barrier at the position where the channel width has a maximum value. When the turntable starts rotating, a flow arises similar to the flow patterns observed in the annular configuration (figure 2), and the two-dimensional turbulent flow resulting from the flow separation at the inner cylinder is seen to become organized into a row of cells filling the channel completely. As in the annular geometry the ultimate size of the cells is determined by the channel width, but since the channel width in the present configuration varies along the channel, it can be expected that also the sizes of the eddies will be different along the channel. Figure 15 shows a typical streakline pattern photographed during the final stage of the spin-up process, and this pattern clearly demonstrates the dependence of the cell size on the local channel width: where the channel narrows the cell size decreases, and vice versa for a widening channel.

4. Conclusions and discussion

Laboratory experiments on the spin-up of a free-surface fluid in a variety of non-axisymmetric geometries have revealed some interesting phenomena not yet reported thus far, and the following conclusions can be formulated.

(i) The relative flow arising instantaneously after starting the turntable has uniform vorticity $\omega = -2\Omega$, and its streamlines $\Psi =$ constant are given by $\nabla^2\Psi = 2\Omega$ with $\Psi = 0$ at the lateral flow boundaries. For the geometries considered in this study, the experimentally observed streamline patterns in the initial stage of the spin-up process show good agreement with the theory. The agreement with theoretical solutions is also confirmed by additional velocity measurements.

(ii) An important feature characterizing the next stage of the spin-up process is the subsequent flow separation occurring at the lateral flow boundaries. This separation is caused by decreasing pressure gradients as well as by vorticity production in the viscous shear layers at the lateral boundaries. In many cases the separation gives rise to irregular three-dimensionally turbulent flow. Observations revealed that such flows become two-dimensional within a few rotation periods – an effect caused by the basic rotation. A common feature of two-dimensional flows is the so-called inverse energy cascade and organization of the flow into larger vortex cells has indeed been observed. This is in marked contrast to the flow arising during the spin-down from rigid-body rotation to rest: although initially the flow is governed by $\nabla^2\Psi = -2\Omega$ with $\Psi = 0$ at the boundaries (leading to the same streamline patterns as for the spin-up, but with reversed flow directions), the flow separation results in a three-dimensionally turbulent flow which remains essentially three-dimensional during its decay (owing to the absence of rotation). As a consequence, no organization into cells is observed during the spin-down. For the spin-up case, the ultimate size of the cells in the 'organized' flow is limited by the lateral flow boundaries, and it can therefore be expected that their number N will depend on the particular geometry. This conjecture has been confirmed by experiments with various flow geometries (different sizes and different shapes).

(iii) Once the flow has become organized into a number of circular cells, the flow pattern shows no drastic changes. In this third stage of the spin-up process the relative flow in each cell decays very slowly as a result of the weak circulation driven by the Ekman layer at the bottom of the cell, in complete analogy with the spin-up or spin-down of fluid confined in a rotating circular cylinder. The experiments revealed that the observed spin-up time corresponds with the well-known Ekman timescale found for the spin-up of a free-surface fluid in an open cylinder.

An important question not yet addressed concerns the effect of the free surface upon the flow during the subsequent stages of the spin-up process. It has been tacitly assumed that the free surface was in all cases approximately horizontal, so that 'topographic' effects were absent. In the laboratory experiments on the spin-up of a fluid in a rectangular tank as described by van Heijst, Davies and Davis (1989), however, it was found that the flexibility of the free surface can induce a translation of vortices, and this may thus affect the flow during the later stages of the spin-up. Van Heijst *et al.* have performed their experiments both for the case of a free-surface fluid and for the case in which the fluid was covered by a flat, rigid lid. As expected, the starting flow was identical in both cases. In the case of a free surface, however, the cyclonic vortices formed during and after the flow separation from the tank walls showed a tendency to slowly drift towards the centre of the tank (which coincided in their experiments with the rotation axis). This behaviour is explained by the mass defect due to the free-surface depression associated with a cyclonic vortex, such that the centrifugal force acting on the fluid column containing the vortex is no longer balanced by the radial pressure gradient. In most of the configurations considered in the previous sections of the present paper such a radial translation has not been observed, simply because the geometry did not allow any large radial excursions. An exception is the semicircle geometry, where the cyclonic vortices arising in the corners of the domain during the flow separation stage (figure 10*b*) are seen to grow and gradually shift to a position nearer to the rotation axis (figure 10*c*, *d*), until they finally merge into a single cyclonic cell (figure 10*e*). This behaviour of the cyclonic vortices would most likely have been different if the experiment was performed with a horizontal rigid lid on top of the fluid.

In the experiments described in this paper the cylinder was in all cases mounted on the turntable such that its symmetry axis coincided with the axis of rotation. Under the assumption that any free-surface elevations or depressions are small compared with the total water depth, it is obvious that the starting flow is independent of the location of the rotation axis: the instantaneously arising relative flow is governed by the relative vorticity, which takes a uniform value of -2Ω over the flow domain, irrespective of the position of the rotation axis. On the other hand, the flow during the later stages of the free-surface spin-up will be affected by the positioning of the axis, because of the translation tendency of free-surface vortices mentioned before. When the fluid is covered with a horizontal rigid lid, however, this tendency is absent and the flow during the various stages of the spin-up would again be entirely independent of the axis position.

The author is grateful to Frans Nieuwstadt and Dirk Visser for some illuminating discussions about the structure of the instantaneously arising flow in the initial stage of the spin-up and its theoretical description, and to Piet Jonker for producing the streamline plots.

REFERENCES

BATCHELOR, G. K. 1969 Computation of the energy spectrum in homogeneous two-dimensional turbulence. *Phys. Fluids* **12** (Suppl. II), 233–240.

BENTON, E. R. & CLARK, A. 1974 Spin-up. *Ann. Rev. Fluid Mech.* **6**, 257–280.

BUZYNA, G. & VERONIS, G. 1971 Spin-up of a stratified fluid: theory and experiment. *J. Fluid Mech.* **50**, 579–608.

GREENSPAN, H. P. & HOWARD, L. N. 1963 On time-dependent motion of a rotating fluid. *J. Fluid Mech.* **17**, 385–404.

HEIJST, G. J. F. VAN, DAVIES, P. A. & DAVIS, R. G. 1989 Spin-up in a rectangular container. *Phys. Fluids.* (submitted).

HOLTON, J. R. 1965 The influence of viscous boundary layers on transient motions in a stratified rotating fluid. Part 1. *J. Atmos. Sci.* **22**, 402–411.

LINDEN, P. F. & HEIJST, G. J. F. VAN 1984 Two-layer spin-up and frontogenesis. *J. Fluid Mech.* **143**, 69–94.

PEDLOSKY, J. 1967 The spin-up of a stratified fluid. *J. Fluid Mech.* **28**, 463–480.

WALIN, G. 1969 Some aspects of time-dependent motion of a stratified rotating fluid. *J. Fluid Mech.* **36**, 289–307.